analytical chemistry

Subscriber access provided by NAGOYA UNIV

Article

A Dual-modal Molecular Probe for Near-infrared Fluorescence and Photoacoustic Imaging of Peroxynitrite

jianjian zhang, Xu Zhen, Jianfeng Zeng, and Kanyi Pu

Anal. Chem., **Just Accepted Manuscript** • DOI: 10.1021/acs.analchem.8b01879 • Publication Date (Web): 26 Jun 2018

Downloaded from http://pubs.acs.org on June 26, 2018

Just Accepted

"Just Accepted" manuscripts have been peer-reviewed and accepted for publication. They are posted online prior to technical editing, formatting for publication and author proofing. The American Chemical Society provides "Just Accepted" as a service to the research community to expedite the dissemination of scientific material as soon as possible after acceptance. "Just Accepted" manuscripts appear in full in PDF format accompanied by an HTML abstract. "Just Accepted" manuscripts have been fully peer reviewed, but should not be considered the official version of record. They are citable by the Digital Object Identifier (DOI®). "Just Accepted" is an optional service offered to authors. Therefore, the "Just Accepted" Web site may not include all articles that will be published in the journal. After a manuscript is technically edited and formatted, it will be removed from the "Just Accepted" Web site and published as an ASAP article. Note that technical editing may introduce minor changes to the manuscript text and/or graphics which could affect content, and all legal disclaimers and ethical guidelines that apply to the journal pertain. ACS cannot be held responsible for errors or consequences arising from the use of information contained in these "Just Accepted" manuscripts.

ACS Publications

is published by the American Chemical Society. 1155 Sixteenth Street N.W., Washington, DC 20036

Published by American Chemical Society. Copyright © American Chemical Society. However, no copyright claim is made to original U.S. Government works, or works produced by employees of any Commonwealth realm Crown government in the course of their duties.

A Dual-modal Molecular Probe for Near-infrared Fluorescence and Photoacoustic Imaging of Peroxynitrite

Jianjian Zhang,[†,‡] **Xu Zhen**,[‡] **Jianfeng Zeng**,[*,§] and **Kanyi Pu**[*,‡]

[†]Key Laboratory of Synthetic and Natural Functional Molecule Chemistry of Ministry of Education, College of Chemistry and Materials Science, Northwest University, Xi'an, Shaanxi 710127, People's Republic of China

[‡]School of Chemical and Biomedical Engineering, Nanyang Technological University, 637457, Singapore.

[§]State key Laboratory of Radiation Medicine and Protection, Soochow University, Suzhou 215123, People's Republic of China

*Corresponding Author: Zeng J., jfzeng@suda.edu.cn; Pu K., kypu@ntu.edu.sg.

ABSTRACT: Peroxynitrite ($ONOO^-$), a reactive and short-lived biological oxidant, is closely related with many pathological conditions such as cancer. However, real-time *in vivo* imaging of $ONOO^-$ in tumor remains to be challenging. Herein, we develop a near-infrared fluorescence (NIRF) and photoacoustic dual-modal molecular probe ($CySO_3CF_3$) composed of a water-soluble hemicyanine dye caged with a trifluoromethyl ketone moiety for *in vivo* imaging of $ONOO^-$. The trifluoromethyl ketone moiety can undergo a series of $ONOO^-$-induced cascade oxidation-elimination reactions, leading to sensitive and specific fluorescence and photoacoustic turn-on responses toward $ONOO^-$; while a zwitterionic structure of the hemicyanine component ensures good water-solubility. $CySO_3CF_3$ thus not only can specifically detect $ONOO^-$ in solution and cells with the limit of detection down to 53 nM, but also allows for NIRF and photoacoustic dual-modal imaging of $ONOO^-$ in the tumor of living mice.

Reaction oxygen and nitrogen species (RONS) play a vital role in physiological and pathological processes of the living system.[1] Peroxynitrite ($ONOO^-$) as a highly reactive RONS can nitrate the biomacromolecules including proteins, nucleic acids and lipids, and disorganize their biological functions,[2] leading to mitochondria malfunction and cellular apoptosis. In tumor microenvironment, $ONOO^-$ is closely related to tumor immunosuppression. Particularly, $ONOO^-$ can nitrate p53 protein,[3] a critical regulator of tumor suppressor protein that is encoded by gene TP53 (tumor protein p53) in human body, which causes the loss of the control role of p53 protein to cell cycle followed by a series of cytotoxic effects, ultimately accelerating the formation of tumor.[4] Thereby, real-time imaging of $ONOO^-$ in tumor is essential for understanding the pathological functions of $ONOO^-$ and developing innovative therapeutic approach to tumor treatment.

Fluorescence imaging has been developed for detection of $ONOO^-$,[5-11] but most of fluorescent probes are only responsive to visible light, which is not ideal for *in vivo* imaging due to shallow tissue penetration. In contrast, photoacoustic (PA) imaging is a hybrid imaging modality that combines laser excitation with acoustic detection, offering higher tissue penetration depth (up to ≈ 5 cm) for *in vivo* imaging.[12-14] Although near-infrared (NIR) molecular dyes,[15,16] polymer nanoparticles,[17-24] fluorescence proteins,[25,26] porphysomes,[27,28] upconversion nanoparticles,[29,30] quantum dots,[31] gold nanoparticles,[32] carbon dots[33] and 2D materials[34] have been used for PA imaging, smart activatable probes with specific PA responses toward $ONOO^-$ are less exploited.[35,36] We recently developed organic semiconducting nanoprobes for ratiometric PA imaging of $ONOO^-$.[37] Although it can be applied for *in vivo* imaging, this nanoprobe was doped with bulky borane in addition to the chromophores to achieve selectivity. Besides, the fluorescence is completely quenched, making it incompatible for fluorescence imaging.

In this study, we report the design and synthesis of a water-soluble small-molecular probe ($CySO_3CF_3$) for *in vivo* near-infrared fluorescence (NIRF)/PA dual-modal imaging of $ONOO^-$. $CySO_3CF_3$ is composed of trifluoromethyl ketone moiety (TFK),[6-8,38] an $ONOO^-$-responsive unit, caged NIR hemicyanine dye with a zwitterionic structure[39] (Scheme 1a). The probe is nonfluorescence because $CySO_3OH$ is in a "caged" state with weak electron-donating ability of the oxygen atom.[37,40-44] In the presence of $ONOO^-$, $CySO_3CF_3$ is converted into the uncaged molecule ($CySO_3OH$) through a series of cascade oxidation-elimination reactions. Due to the enhanced electron-donating ability from the oxygen atom in $CySO_3OH$, such an $ONOO^-$-induced conversion results in not only fluorescent turn-on but also red-shifted NIR absorption, enabling NIRF/PA dual-modal imaging.

EXPERIMENTAL SECTION

Chemicals. All chemicals and reagents were obtained from Sigma-Aldrich unless otherwise stated. Sodium hypochlorite (NaOCl, 5% aqueous solution). Hydrogen peroxide (H_2O_2, 30% aqueous solution), sodium nitrite ($NaNO_2$) and

boron tribromide (BBr_3) were purchased from TCI (Tokyo, Japan). Anhydrous dichloromethane (CH_2Cl_2) were treated with CaH_2 under reflux for 24 h and redistilled before use. Milli-Q water was supplied by Milli-Q Plus System (MilliporeCorporation, Breford, U.S.A.). A stock solution (1 mmol/L) of $CySO_3CF_3$ was prepared by dissolving in dimethyl sulphoxide (DMSO).

Instrumentation. UV–vis spectra were recorded on a Shimadzu UV-2450 spectrophotometer. Fluorescence spectra were recorded on a Fluorolog 3-TCSPC spectrofluorometer (Horiba Jobin Yvon). NMR spectra were measured using a Bruker 300 MHz instruments (Germany). All ^1H chemical shifts (δ) are relative to residual protic solvent ($CHCl_3$: δ 7.26 ppm). Mass spectra were measured using Thermo LCQ Fleet LC-MS with ESI mode (America). The pH values were measured using a digital pH-meter (Seven-Compact S220, Zurich, Switzerland). High performance liquid chromatography (HPLC) analyses were performed on an Agilent 1260 system equipped with a G1311B pump, UV detector and an Agilent Zorbax SB-C18 RP (9.4 × 250 mm) column, with CH_3CN (0.1% of TFA) and water (0.1% of TFA) as the eluent. Fluorescence images of cells were acquired on Laser Scanning Microscope LSM800 (Zeiss) or LX71-inverted fluorescence microscope (Olympus) with Retiga-2000R CCD camera. Fluorescence images of tumor were acquired with IVIS Spectrum imaging system (PerkinElmer, Inc.). *In vivo* PA images were performed with a Multispectral Optoacoustic Tomography scanner (MSOT, iThera medical, Germany) with excitation light of 680-850 nm.

Synthesis

Compound 4: To a solution of 3-(4-methoxyphenyl) propanoic acid (**3**, 2.7 g, 15.0 mmol) in ethanol (20 mL) was added H_2SO_4 (0.7 mL, con.) at room temperature under nitrogen atmosphere. The resulting mixture was refluxed for 4 h. Then ethanol was evaporated under reduced pressure, and the residue was added ethyl acetate (60 mL). The resulting solution was washed with H_2O (3 × 50 mL), saturated sodium bicarbonate (30 mL) and saturated sodium chloride (30 mL), respectively. The organic phase was dried with anhydrous Na_2SO_4, and then concentrated under reduced pressure, which obtained ethyl 3-(4-methoxyphenyl)propanoate **4** (2.99 g, yield 96%) without purification. ^1H NMR (300 MHz, $CDCl_3$): δ = 7.12 (d, *J* = 8.6 Hz, 2 H), 6.83 (d, *J* = 8.7 Hz, 2 H), 4.12 (q, *J* = 7.1 Hz, 2 H), 3.78 (s, 3 H), 2.89 (d, *J* = 7.8 Hz, 2 H), 2.58 (d, *J* = 7.8 Hz, 2 H), 1.23 (t, *J* = 7.2 Hz, 3 H). MS (ESI): *m/z* = 209.13 $[M+H]^+$.

Compound 5: To a solution of ethyl 3-(4-methoxyphenyl) propanoate **4** (2.91 g, 14.0 mmol) and $TMSCF_3$ (3.1 mL, 21.0 mmol) in tetrahydrofuran (THF, 10 mL) was added CsF (21.2 mg, 0.14 mmol). The mixture was stirred at room temperature under nitrogen atmosphere for 18 h and then CH_2Cl_2 (30 mL) was added to the resulting solution, the mixture was treated with water (3 × 10 mL) and saturated sodium chloride (10 mL) respectively. The organic phase was dried with anhydrous Na_2SO_4, and then was concentrated under reduced pressure. The residue was purified by silica gel column chromatography (ethyl acetate/hexane, 5%) to afford the desired product (2-ethoxy-1,1,1-trifluoro-4-(4-methoxyphenyl) butan-2-yl)trimethylsilane **5**. (4.02 g, yield 86%). ^1H NMR (300 MHz, $CDCl_3$): δ = 7.14 (d, *J* = 8.2 Hz, 2 H), 6.86 (d, *J* = 8.0 Hz, 2 H), 3.81 (s, 3 H), 3.81-3.56 (m, 2 H), 2.78-2.63 (m, 2 H), 2.18-1.96 (m, 2 H), 1.26 (td, *J* = 7.0, 0.9 Hz, 3 H), 0.24 (d, *J* = 0.9 Hz, 9 H). MS (ESI): *m/z* = 335.19 $[M+H]^+$.

Compound 6: To a solution of compound **5** (4.0 g, 12 mmol) in THF (2 mL) was added TBAF (1 M in THF, 13.0 mL) dropwise under nitrogen atmosphere. The mixture was stirred at room temperature for 5 h and then was treated with hydrochloric acid (4.0 M, 4.0 mL) for 3 h. CH_2Cl_2 (30 mL) was added to the resulting solution, which was washed with water and saturated sodium chloride respectively. The organic phase was dried with anhydrous Na_2SO_4, and then was concentrated under reduced pressure. The residue was purified by silica gel column chromatography (ethyl acetate/hexane, 5%) to obtain trifluoro-4-(4-methoxyphenyl)butan-2-one **6**. (2.45 g, yield: 88%);^1H NMR (300 MHz, $CDCl_3$): δ = 7.11 (d, *J* = 8.7 Hz, 2 H), 6.84 (d, *J* = 8.7 Hz, 2 H), 3.78 (s, 3 H), 3.05-2.98 (m, 2 H), 2.96-2.89 (m, 2 H). MS (ESI): *m/z* = 233.09 $[M+H]^+$.

Compound 7: To a solution of 1,1,1-trifluoro-4-(4-methoxyphenyl) butan-2-one **6** (2.4 g, 10.3 mmol) in CH_2Cl_2 (20 mL) was added BBr_3 (5.2 mL, 13.4 mmol) at –78 °C under nitrogen atmosphere. The resulting mixture was then warmed to room temperature and stirred 12 h. Then ice-water was added slowly, and the mixture was added ethyl acetate (50 mL). The resulting solution was washed with H_2O (3 × 20 mL), saturated sodium bicarbonate (30 mL) and saturated sodium chloride (30 mL), respectively. The organic phase was dried with anhydrous Na_2SO_4, and then concentrated under reduced pressure, which was purified by silica gel column chromatography (ethyl acetate/hexane, 25%) to obtain 1,1,1-trifluoro-4-(4-hydroxyphenyl)butan-2-one **7** (1.84 g, yield 82%); ^1H NMR (300 MHz, $CDCl_3$): δ = 7.06 (d, *J* = 8.6 Hz, 2 H), 6.77 (d, *J* = 8.6 Hz, 2 H), 3.05-2.97 (m, 2 H), 2.95-2.80 (m, 2 H). MS (ESI): *m/z* = 219.16 $[M+H]^+$.

$CySO_3Cl$: A mixture of compound **1** (516 mg, 3.0 mmol), compound **2** (1.76 g, 6.0 mmol) and sodium acetate (246 mg, 3.0 mmol) were dissolved in acetic anhydride (20.0 mL) under nitrogen atmosphere and heated to 90 °C for 1 h with a Dean-Stark condenser. After cooling to room temperature, the resulting green solid was collected, washed with Et_2O (100 mL) and purified by silica gel column chromatography using CH_2Cl_2/ 0-2% methanol as eluent to afford desired product **$CySO_3Cl$** as a blue solid. Yield: 1.59 g (73%). ^1H NMR (300 MHz, $CDCl_3$): δ = 8.43 (d, *J* = 14.2 Hz, 2H), 7.52 (d, *J* = 7.2 Hz, 2H), 7.48-7.32 (m, 4H), 7.28 (d, *J* = 7.0 Hz, 2H), 6.34 (d, *J* = 14.1, 2H), 4.23 (t, *J* = 7.2 Hz, 2H), 2.90 (t, *J* = 6.6 Hz, 2H), 2.75 (t, *J* = 4.2 Hz, 2H), 2.08-1.88 (s, 10H), 1.73 (s, 12H) ppm; ESI-MS, m/z: 727.48 $[M]^+$.

$CySO_3OH$: To a stirred solution of resorcinol (220 mg, 2.0 mmol) in acetonitrile (ACN, 15 mL) was added K_2CO_3 (276 mg, 2.0 mmol) at room temperature under nitrogen atmosphere and the resulting mixture was stirred for 20 min. Then, a solution of $CySO_3Cl$ (727 mg, 1.0 mmol) in DMF (10 mL) was added to the above mixture via a syringe, and the reaction mixture was heated at 50 °C for 4 h. Eventually the solvent was evaporated under reduced pressure, and the crude product was purified by flash column chromatography (petroleum ether/CH_2Cl_2/MeOH = 25:25:1) on silica gel, affording the desired compound **$CySO_3OH$** as a blue-green solid (400 mg, yield 79%). ^1H NMR (400 MHz, $CDCl_3$): *δ* = 8.75 (d, *J* = 14.8 Hz, 1H), 7.63

(d, *J* = 14.8 Hz, 1H), 7.51-7.57 (m, 2H), 7.45-7.39 (m, 3H), 6.87-6.82 (m, 2H), 6.51 (d, *J* = 14.8 Hz, 1H), 4.37 (t, *J* = 7.2 Hz, 2H), 2.91 (t, *J* = 7.2 Hz, 2H), 2.78-2.72 (m, 4H), 2.11-2.05 (m, 2H), 1.99-1.92 (m, 4H), 1.81 (s, 6H) ppm; ESI-MS, m/z: 506.38 $[M]^+$.

$CySO_3CF_3$: To a stirred solution of BTC (17.8 mg, 0.06 mmol) dissolved in dichloromethane (1 ml) and cooled to 0 °C, was added drop-wise a solution of the compound **7** (17.4 mg, 0.08 mmol) in dichloromethane (2.0 ml) and then triethylamine (8.0 mg, 0.08 mol) was added. During addition, the temperature was kept at 0 °C. After the addition was completed, the mixture was allowed slowly to rise to room temperature and stirring was continued for 2h. Then a solution of $CySO_3OH$ (30 mg, 0.06 mmol) in dichloromethane (2 ml) was added to the above mixture and stirred 30 min. The resulting mixture was concentrated under vacuum, which was purified by silica gel column chromatography (ethyl acetate/hexane, 10%) to obtain **$CySO_3CF_3$** (14.0 mg, yield 31%). ^{1}H NMR (300 MHz, CD_3OD): δ = 8.64 (d, *J* = 19.6 Hz, 1H), 7.52-7.39 (m, 5H), 7.42-7.35 (m, 5H), 6.92 (d, *J* = 7.2 Hz, 1H), 6.89 (s, 1H), 6.43 (d, *J* = 19.6 Hz, 1H), 4.27 (t, *J* = 8.8 Hz, 2H), 3.25-3.05 (m, 4H), 2.90 (t, *J* = 9.2 Hz, 2H), 2.73 (t, *J* = 8.0 Hz, 2H), 2.68 (t, *J* = 8.2 Hz, 2H), 2.11-1.85 (m, 6H), 1.77 (s, 6H). ^{19}F NMR (300 M, CD_3OD): = -79.28. MS (ESI): *m/z* = 750.49 $[M]^+$.

Cell Culture and Cytotoxicity Test. HeLa (Human Cervical Adenocarcinoma Epithelial Cells), RAW 264.7 (Mouse Leukaemic Monocyte Macrophage Cell Line) and NIH 3T3 (Mouse Embryonic Fibroblasts) cells were purchased from the American Type Culture Collection (ATCC). These three kinds of the cells were cultured in DMEM (Dulbecco's Modified Eagle Medium) supplemented with heat-inactivated fetal bovine serum (10%) in a humidified environment containing 5% CO_2 and 95% air at 37 °C, respectively. Cells were seeded in 96 well plates (1×10^4 cells/well) for 24 h, and then $CySO_3CF_3$ (final concentration 0, 5, 10, 20, 35, 50, and 80 μmol/L) was added to the cell culture medium. The corresponding cells were incubated with or without (control) $CySO_3CF_3$ for 24 h, followed by the addition of MTS (100 μL, 0.1 mg/mL) for 4 h. The absorbance of MTS at 490 nm was measured by using a microplate reader. The cytotoxic effect (VR) of $CySO_3CF_3$ were assessed using the following equation: $VR = A/A_0 \times 100\%$, where A and A_0 are the absorbance of the experimental group and control group, respectively. The assays were performed in six sets for each concentration.

Cell Imaging. After seeded RAW 264.7 cells reached 70–90% confluency, the cells were washed three times using prewarmed PBS buffer (10 mM, pH 7.4). Then the cells were incubated with $CySO_3CF_3$ in an atmosphere of 5% CO_2 and 95% humidified air at 37 °C for 30 min. After that the cells were stained with 4',6-diamidino-2-phenylindole (DAPI) (NucBlue Live ReadyProbes Reagent, Thermo Fisher) for the nuclei as protocols. Fluorescence images of the live cells were taken with the wide-field fluorescence microscope Leica DMi8 (Leica, Germany) equipped with scientific CMOS (sCOMS, Hamamatsu, Japan). Excitation/emission wavelengths were 405/490 ± 20 nm for DAPI, and 680/710 ± 20 nm for $CySO_3CF_3$.

Tumor Mouse Model. All animal experiments were performed under protocols approved by the Laboratory Animal Center of Soochow University. To establish tumors in 6-week-old female nude mice, 2 million 4T1 cells suspended in 1 mL DMEM (containing 10% fetal bovine serum, 1% penstrep, 100 U/mL penicillin, and 100 μg/mL streptomycin) were injected subcutaneously near the armpits of the mouse. Tumors were grown until a single aspect was ~7 mm (approximately 10–15 days) before used for fluorescence and PA imaging.

***In Vivo* Fluorescence Imaging.** Nude mice bearing 4T1 tumors were injected with $CySO_3CF_3$ (50 μM in 100 μL saline) (n = 3) through the tail vein using a microsyringe. Fluorescence imaging were performed on the IVIS spectrum imaging system at designated time points after $CySO_3CF_3$ administration (ex: 675 ± 10 nm, em: 720 ± 10 nm). Images quantitation was performed using Living Image software for IVIS imaging system.

***In Vivo* Photoacoustic Imaging**. After the nude mice were anesthetized using 2% isoflurane in oxygen, $CySO_3CF_3$ (50 μM in 100 μL saline) (n = 3) was systematically injected through the tail vein using a microsyringe. Multispectral Optoacoustic Tomography scanner was used to acquire the PA images at 680 nm after systematical administration of $CySO_3CF_3$. *In vivo* PA spectra with excitation light from 680 to 850 nm were acquired from the tumor regions after 3 h systemic administration of $CySO_3CF_3$.

Data Analysis. The fluorescence data were measured by region of interest (ROI) analysis using Living Image 4.0 Software. *In vivo* and ex vivo PA intensities were quantified with ROI analysis using postprocessing software ViewMSOT. Results were expressed as the mean ± standard deviations (SD) unless otherwise stated.

RESULTS AND DISCUSSION

Scheme 1b describes the synthesis route of $CySO_3CF_3$. (Z)-2-chloro-3-(hydroxymethylene)cyclohex-1-enecarbaldehyde **1** was first reacted with 2,3,3-trimethyl-1-(4-sulfobutyl)-3H-indol-1-ium **2** to afford compound $CySO_3Cl$, followed by reacted with resorcinol in the existence of K_2CO_3 to obtain $CySO_3OH$ directly for the following reaction. The other component, the esterified ethyl 3-(4-methoxyphenyl) propanoate was firstly attacked by (Trifluoromethyl)trimethylsilane ($TMSCF_3$) and then eliminated to form compound **6**, which was further treated with BBr_3 to afford compound **7**. Finally, the oxygen atom of compound $CySO_3OH$ was caged with compound **7** using phosgene to afford $CySO_3CF_3$. The chemical structure of $CySO_3CF_3$ was characterized by proton nuclear magnetic resonance (^{1}H NMR) and electrospray ionization-mass spectrometry (ESI-MS), as shown in the Experimental Section and in the Supporting Information.

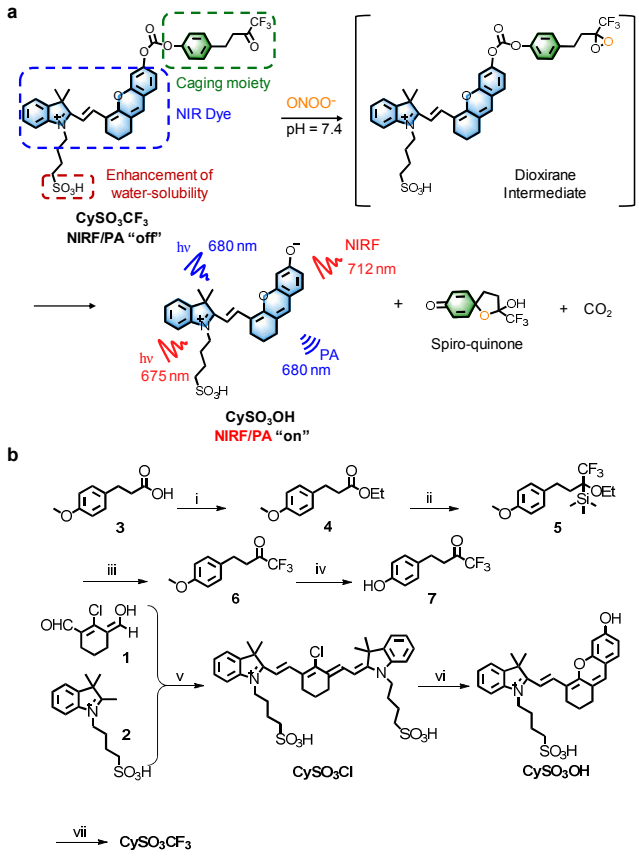

Scheme 1. Sensing mechanism and synthetic scheme. a) Schematic illustration of peroxynitrite-induced oxidation of a trifluoromethyl ketone moiety *via* a dioxirane intermediate. b) Syntheses of $CySO_3CF_3$. Reagents and conditions: (i) H_2SO_4 (con.), reflux, 4 h, EtOH, 96%; (ii) $TMSCF_3$, CsF, THF, 18 h, 86%; (iii) tetrabutylammonium fluoride (TBAF), THF, 5 h, then 4 M HCl, 3 h, 88%; (iv) BBr_3, -78 °C, room temperature, 12 h, CH_2Cl_2, 82%; (v) sodium acetate, acetic anhydride, 90 °C, 1 h, 73%; (vi) resorcinol, K_2CO_3, DMF, 50 °C, 4 h, 79%; (vii) **7**, triphosgene, Et_3N, 0 °C, 2 h, anhydrous CH_2Cl_2, 31%.

To validate $ONOO^-$-induced oxidation of $CySO_3CF_3$, high performance liquid chromatography (HPLC) analysis was conducted (Figure S1, Supporting Information). The data showed that $CySO_3CF_3$ (HPLC retention time, T_R = 8.7 min) was converted to $CySO_3OH$ (T_R = 4.6 min). The ESI spectrometry analysis (Figure S2, Supporting Information) of the probe treated with $ONOO^-$ further confirmed the formation of the expected $CySO_3OH$ (m/z 506.38) and the desired spiro-quinone (m/z 234.05). The reaction mechanism was confirmed by the NMR spectra using trifluoro-(4-methoxyphenyl)butan-2-one as a model compound (Figure S3, Supporting Information).

To study the optical response along with $ONOO^-$-induced cleavage, the spectroscopic properties of $CySO_3CF_3$ under physiological conditions (1×PBS: phosphate buffer, pH 7.4) were measured before and after addition $ONOO^-$. $CySO_3CF_3$ intrinsically had the absorption maximum at 602 nm (Figure 1a); upon addition of $ONOO^-$, this peak gradually decreased, while a new peak at 686 nm appeared (Figure S4, Supporting Information). At the saturation point, the absorbance at 686 nm for $CySO_3CF_3$ was 0.48, which was 9.4-fold higher than that at the initial state (0.051). In addition, the fluorescence at 712 nm dramatically enhanced upon addition of $ONOO^-$ (Figure S5, Supporting Information), which was ~59-fold higher relative to its initial state at the saturation point. Such absorption and fluorescent responses confirmed the $ONOO^-$-induced conversion as proposed in Scheme 1. Both absorption and fluorescent signals had good linearity with the concentration of $ONOO^-$ (Figure 1b and Figure S6, Supporting Information), showing the limits of detection of 115 and 53 nM, respectively.

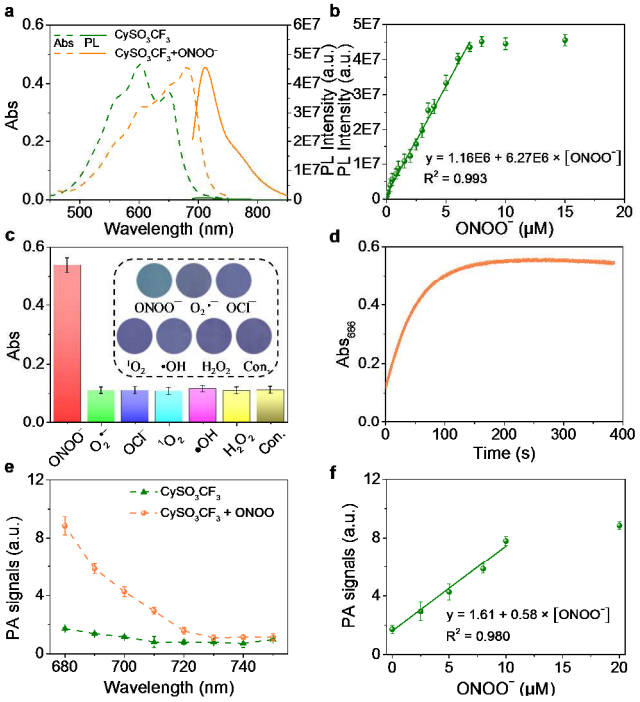

Figure 1. In vitro characterization. a) UV–vis absorption (dash line) and fluorescence (solid line) spectra of $CySO_3CF_3$ (5 μM) in the absence or presence of $ONOO^-$ (15 μM) for 3 min in PBS buffer (10 mM, pH 7.4). Excitation: 675 nm. b) Fluorescence intensities of $CySO_3CF_3$ (5 μM) as a function of the concentration of $ONOO^-$ in PBS buffer (10 mM, pH 7.4) (relative standard deviation δ = 1.16E5, n = 3; slope, 6.27E6). c) UV–vis absorption of $CySO_3CF_3$ (5 μM) after incubation with indicated ROS for 3 min. Inset: white light images of $CySO_3CF_3$ (5 μM) in the absence or presence of ROS for 3 min in PBS buffer (10 mM, pH 7.4). d) Ab_{686} of $CySO_3CF_3$ (5 μM) as a function of time in the presence of $ONOO^-$ (15 μM) in PBS buffer (10 mM, pH 7.4). e) PA spectra of $CySO_3CF_3$ (5 μM) before and after addition of $ONOO^-$ in PBS buffer (10 mM, pH 7.4). f) PA_{686} of $CySO_3CF_3$ (5 μM) as a function of the concentration of $ONOO^-$ in PBS buffer (10 mM, pH 7.4) (relative standard deviation δ = 0.028, n = 3; slope, 0.58). The error bars represent standard deviations of three separate measurements.

The specificity of $CySO_3CF_3$ towards $ONOO^-$ was tested against other RONS ($O_2^{\bullet-}$, ClO^-, $^1O_2$, •OH, H_2O_2, NO, NO_2^-) and sulphur compounds (S^{2-}, GSH, Cys, Hcy, HSO_3^-, SO_3^{2-}). The results showed that other RONSs and sulphur compounds could not induce any absorption and fluorescent changes for the probe (Figure 1c and Figure S7, Supporting Information). Thus, $CySO_3CF_3$ could only be activated by $ONOO^-$, changing their solution colors from purple to cyan (the inset of Figure 1c). To determine the activation speed of the probe, the reaction kinetics of $CySO_3CF_3$ with $ONOO^-$

was studied by time-course absorption measurements (Figure 1d and Figure S8, Supporting Information). The corresponding pseudo-first-order rate constant (k) for the present $ONOO^-$ reaction was determined to be 1.49×10^3 $M^{-1}s^{-1}$. Thus, $CySO_3CF_3$ should be able to specifically detect $ONOO^-$ in real time.

The PA sensing ability of $CySO_3CF_3$ was also tested under physiological conditions. After activation by $ONOO^-$, the PA band ranging from 680 to 750 nm appeared (Figure 1e), consistent with the absorption response. At the saturation point, the PA intensity at 680 nm (PA_{680}) was 5.1-fold higher than that at the initial state (1.73). In contrast, in the present of other ROS ($O_2^{\bullet-}$, ClO^-, $^1O_2$, $\bullet OH$, and H_2O_2), no obvious changes were observed in the PA spectra (Figure S9, Supporting Information). Furthermore, PA_{680} was linearly correlated to the concentration of $ONOO^-$ with the limit of detection of 145 nM, which was closed to that for absorption response. As the concentration of $ONOO^-$ is in the range of 50-100 μM per minute in living systems,[45] $CySO_3CF_3$ should be ideal for sensing $ONOO^-$ in living cells and mice.

The low pH (pH 6.8) of tumor tissues was caused by the highly acidic metabolites, e.g. lactic acid produced by anaerobic glycolysis in the absence of oxygen during tumor growth. To validate the feasibility of probe activation in the acidic tumor environment, the absorption responses of $CySO_3CF_3$ toward $ONOO^-$ was tested at pH ranging from 9.0 to 5.0. The probe presented weakened absorption signals at 686 nm especially when pH decreased from 9.0 to 6.0 (Figure S10, Supporting Information). This could be ascribed to the protonation of the phenoxide product to its conjugate acid at low pH as CySO3OH has pK_a = 7.11. The maximum absorption signals at 600 nm of the conjugate acid were the same as the initially unactivated state. Note that at pH = 6.8, in the present of $ONOO^-$, the absorption value at 686 nm was ≈ 0.290, 3.6-fold higher when compared with its original state (0.081). Hence, despite its pH response, $CySO_3CF_3$ could be applied to fluorescence and PA imaging of $ONOO^-$ in acidic tumor microenvironments.

To validate the reactivity of $CySO_3CF_3$ toward $ONOO^-$ in cells, Fluorescence imaging was conducted on murine macrophage (RAW 264.7) cells (Figure 2a). After incubation with $CySO_3CF_3$ for 30 min, the cells were washed and stained with nuclei indicator, 4',6-diamidino-2-phenylindole (DAPI), which was depicted in blue colors. Images showed a remarkable red fluorescence in the cytoplasm, which implied that the probe underwent a cascade oxidation-elimination reaction with intracellular $ONOO^-$. In contrast, the cells pretreated with *N*-acetylcysteine (NAC), an effective RONS scavenger, only showed weak fluorescence signals. Moreover, the cytotoxicity of $CySO_3CF_3$ was investigated by MTS assay. As shown in Figure 2c and Figure S11 (Supporting Information), the cells including HeLa, RAW 264.7 and NIH 3T3 kept high survival rate upon exposure to $CySO_3CF_3$ with concentrations below 50 μM. These results illustrated that $CySO_3CF_3$ could detect endogenous $ONOO^-$ in living cells and thus had a potential for imaging application.

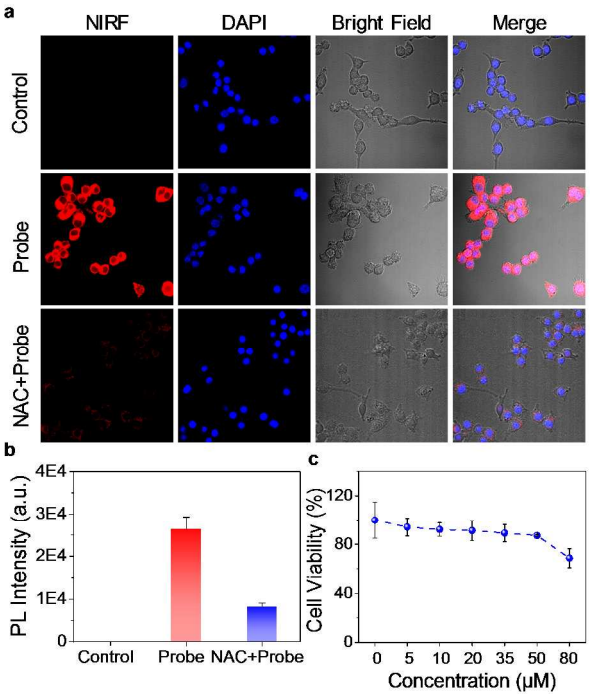

Figure 2. Imaging $ONOO^-$ in cells. a) Confocal microscope fluorescence images of live murine macrophages (RAW 264.7). Cells successively treated with or without NAC (30 min) and then $CySO_3CF_3$ (30 min), [$CySO_3CF_3$] = 10 μM; [NAC] = 1 mM. b) Quantification of fluorescence intensities of RAW 264.7 cells incubated with $CySO_3CF_3$ and other reagents corresponding to Figure 2a. The error bars represent the standard deviation from three separate measurements. c) MTS assay for the survival rate of RAW 264.7 cells treated with various concentrations (0, 5, 10, 25, 35, 50, 80 μM) of $CySO_3CF_3$ for 24 h. Error bars represent the standard deviations of 6 trials.

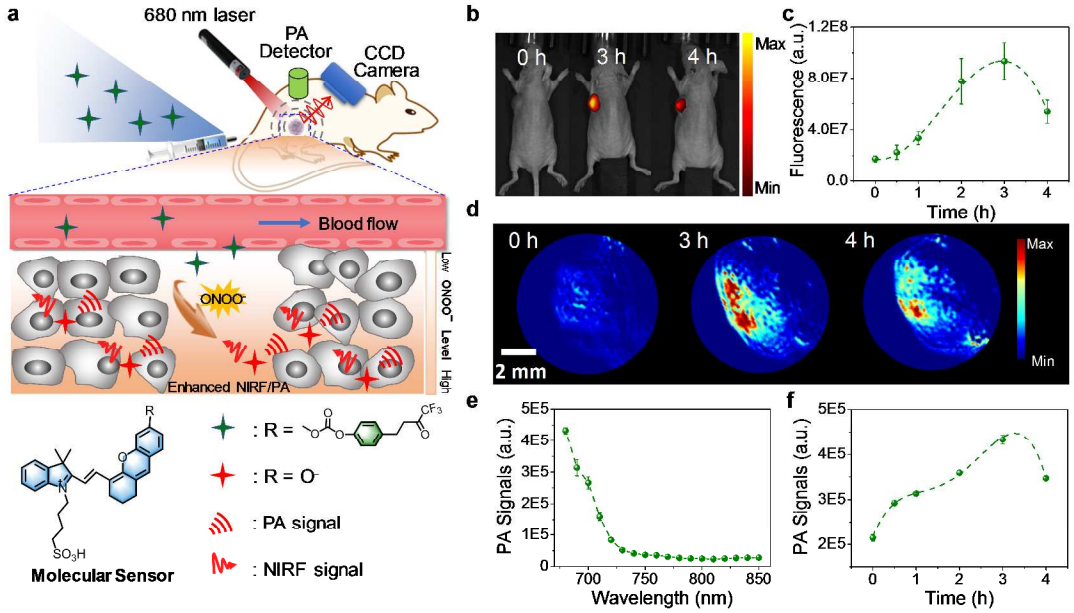

Figure 3. *In vivo* NIRF and PA imaging of $ONOO^-$ using $CySO_3CF_3$. a) Illustration of the mechanism for NIRF and PA imaging of $ONOO^-$ in tumor using $CySO_3CF_3$. $CySO_3CF_3$ first accumulates into tumor and then is activated by $ONOO^-$ through cascade oxidation-elimination reactions, eventually resulting in enhanced NIRF/PA signals. b) Real-time fluorescence imaging of tumor bearing mouse after systemic administration of $CySO_3CF_3$ (50 μM in 100 μL saline) at 0, 3, and 4 h. c) Fluorescence intensity in tumor area as a function of post-injection time for $CySO_3CF_3$ intravenous injected mice. d) Representative PA maximum imaging projection (MIP) of tumor from a systemic administration of a living mouse at 0, 3, and 4 h post-injection of $CySO_3CF_3$ (50 μM in 100 μL saline). e) *In vivo* real-time PA spectra extracted from the tumors in living mice after systemic administration of $CySO_3CF_3$ via intravenous injection for 3 h. f) PA intensity in tumor area as a function of post-injection time for $CySO_3CF_3$ intravenous injection. Error bars represent standard deviations of three separate measurements (n = 3).

The feasibility of using $CySO_3CF_3$ as a NIRF/PA probe to monitor $ONOO^-$ in the subcutaneous 4T1 xenograft tumor of living mice was tested (Figure 3). After systemic administration of $CySO_3CF_3$ into tumor-bearing living mice through tail vein, both NIRF and PA images were longitudinally recorded and quantified. The NIRF and PA signals gradually enhanced for $CySO_3CF_3$-treated mice and reached its maxima 3 h post-injection (Figure 3b, 3d). This showed that the probe was accumulated in the tumor, which was also confirmed by *ex vivo* data (Figure S12, Supporting Information). At t =3 h, the PA and fluorescence intensities of $CySO_3CF_3$-treated tumor were respectively 2.1 and 5.3-fold higher than the background signals of tumor (Figure 3c). The higher signal-to-noise ratio of fluorescence imaging relative to PA imaging has been reported before[19,46-51], which should be mainly ascribed to the better sensitivity of fluorescence imaging and higher tissue background for PA background at 680 nm from hemoglobin. The real-time *in vivo* PA spectra extracted from the tumor regions at t = 3 h showed a strong signal at 680 nm (Figure 3e); Moreover, the PA spectral profile resembled the solution spectrum of activated $CySO_3CF_3$. These results thus not only confirmed the selective activation of $CySO_3CF_3$ by $ONOO^-$ in tumor but also highlighted its ability for both NIRF and PA imaging.

CONCLUSIONS

In summary, we synthesized a water-soluble small-molecular probe ($CySO_3CF_3$) that can be specifically activated by endogenously overexpressed $ONOO^-$ to turn on both NIRF and PA signals. $CySO_3CF_3$ is different from the most reported RONS PA probes which are nanoparticles.[32,43,44] $CySO_3CF_3$ also showed higher NIRF (59-fold) and PA (5.1-fold) enhancement and fast activation kinetics in response to $ONOO^-$. With its zwitterionic structure, $CySO_3CF_3$ has good water-solubility and can be systemically injected into living mice for NIRF and PA dual-modal imaging of $ONOO^-$. To the best of our knowledge, this work represents the first smart molecular probe that detects endogenous $ONOO^-$ in living system with NIRF and PA dual-modal imaging.

ASSOCIATED CONTENT

Supporting Information

The Supporting Information is available free of charge on the ACS Publications website. at DOI: 10.1021/acs.analchem.xxxxxxx.
Additional information as noted in the text (Figures S1–S13); Synthesis, characteristic (^{1}H NMR and MS spectra), UV-Vis absorption, fluorescence and photoacoustic spectra. (PDF)

AUTHOR INFORMATION

Corresponding Author

*E-mail: kypu@ntu.edu.sg
*E-mail: jfzeng@suda.edu.cn

ORCID

Jianjian Zhang: 0000-0002-5220-1280
Kanyi Pu: 0000-0002-8064-6009

Notes

The authors declare no competing financial interest.

ACKNOWLEDGMENT

K.P. thanks Nanyang Technological University (Start-Up grant: NTUSUG: M4081627.120) and Singapore Ministry of Education (Academic Research Fund Tier 1: RG133/15 M4011559 and 2015-T1-002-091; and Tier 2 MOE2016-T2-1-098) for the financial support.

REFERENCES

(1) Nathan, C.; Cunningham-Bussel, A. *Nat. Rev. Immunol.* **2013**, *13*, 349-361.

(2) Alvarez, B.; Radi, R. *Amino Acids* **2003**, *25*, 295-311.

(3) Cobbs, C. S.; Samanta, M.; Harkins, L. E.; Gillespie, G. Y.; Merrick, B. A.; MacMillan-Crow, L. A. *Arch. Biochem. Biophys.* **2001**, *394*, 167-172.

(4) Cobbs, C. S.; Whisenhunt, T. R.; Wesemann, D. R.; Harkins, L. E.; Van Meir, E. G.; Samanta, M. *Cancer Res.* **2003**, *63*, 8670-8673.

(5) Chen, Z.-J.; Ren, W.; Wright, Q. E.; Ai, H.-W. *J. Am. Chem. Soc.* **2013**, *135*, 14940-14943.

(6) Yang, D.; Wang, H.-L.; Sun, Z.-N.; Chung, N.-W.; Shen, J.-G. *J. Am. Chem. Soc.* **2006**, *128*, 6004-6005.

(7) Sun, Z.-N.; Wang, H.-L.; Liu, F.-Q.; Chen, Y.; Tam, P. K. H.; Yang, D. *Org. Lett.* **2009**, *11*, 1887-1890.

(8) Peng, T.; Yang, D. *Org. Lett.* **2010**, *12*, 4932-4935.

(9) Sedgwick, A. C.; Han, H.-H.; Gardiner, J. E.; Bull, S. D.; He, X.-P.; James, T. D. *Chem. Sci.* **2018**, *9*, 3672-3676.

(10) Li, H.; Li, X.; Wu, X.; Shi, W.; Ma, H. *Analy. Chem.* **2017**, *89*, 5519-5525.

(11) Ashton, T. D.; Jolliffe, K. A.; Pfeffer, F. M. *Chem. Soc. Rev.* **2015**, *44*, 4547-4595.

(12) Wang, L. V.; Hu, S. *Science* **2012**, *335*, 1458-1462.

(13) Nie, L.; Chen, X. *Chem. Soc. Rev.* **2014**, *43*, 7132-7170.

(14) Kim, C.; Favazza, C.; Wang, L. V. *Chem. Rev.* **2010**, *110*, 2756-2782.

(15) Kim, C.; Song, K. H.; Gao, F.; Wang, L. V. *Radiology* **2010**, *255*, 442-450.

(16) Roberts, S.; Seeger, M.; Jiang, Y.; Mishra, A.; Sigmund, F.; Stelzl, A.; Lauri, A.; Symvoulidis, P.; Rolbieski, H.; Preller, M.; Deán-Ben, X. L.; Razansky, D.; Orschmann, T.; Desbordes, S. C.; Vetschera, P.; Bach, T.; Ntziachristos, V.; Westmeyer, G. G. *J. Am. Chem. Soc.* **2018**, *140*, 2718-2721.

(17) Gong, H.; Dong, Z.; Liu, Y.; Yin, S.; Cheng, L.; Xi, W.; Xiang, J.; Liu, K.; Li, Y.; Liu, Z. *Adv. Funct. Mater.* **2014**, *24*, 6492-6502.

(18) Pu, K.; Shuhendler, A. J.; Jokerst, J. V.; Mei, J.; Gambhir, S. S.; Bao, Z.; Rao, J. *Nat. Nanotechnol.* **2014**, *9*, 233-239.

(19) Xie, C.; Zhen, X.; Lei, Q.; Ni, R.; Pu, K. *Adv. Funct. Mater.* **2017**, *27*, 1605397.

(20) Lyu, Y.; Zhen, X.; Miao, Y.; Pu, K. *ACS Nano* **2017**, *11*, 358-367.

(21) Sheng, D.; Liu, T.; Deng, L.; Zhang, L.; Li, X.; Xu, J.; Hao, L.; Li, P.; Ran, H.; Chen, H.; Wang, Z. *Biomaterials* **2018**, *165*, 1-13.

(22) Cui, D.; Xie, C.; Pu, K. *Macromol. Rapid Commun.* **2017**, *38*, 1700125.

(23) Jiang, Y.; Pu, K. *Small* **2017**, *13*, 1700710.

(24) Xie, C.; Cheng P.; Pu, K. *Chem.-Eur. J.* **2018**, DOI: 10.1002/chem.201705716.

(25) Razansky, D.; Distel, M.; Vinegoni, C.; Ma, R.; Perrimon, N.; Köster, R. W.; Ntziachristos, V. *Nat. Photonics* **2009**, *3*, 412-417.

(26) Filonov, G. S.; Piatkevich, K. D.; Ting, L.-M.; Zhang, J.; Kim, K.; Verkhusha, V. V. *Nat. Biotechnol.* **2011**, *29*, 757-761.

(27) Lovell, J. F.; Jin, C. S.; Huynh, E.; Jin, H.; Kim, C.; Rubinstein, J. L.; Chan, W. C.; Cao, W.; Wang, L. V.; Zheng, G. *Nat. Mater.* **2011**, *10*, 324-332.

(28) Muhanna, N.; Jin, C. S.; Huynh, E.; Chan, H.; Qiu, Y.; Jiang, W.; Cui, L.; Burgess, L.; Akens, M. K.; Chen, J.; Irish, J.; Zheng, G. *Theranostics* **2015**, *5*, 1428-1443.

(29) Liu, Y.; Kang, N.; Lv, J.; Zhou, Z.; Zhao, Q.; Ma, L.; Chen, Z.; Ren, L.; Nie, L. *Adv. Mater.* **2016**, *28*, 6411-6419.

(30) Lv, R.; Wang, D.; Xiao, L.; Chen, G.; Xia, J.; Prasad, P. N. *Sci. Rep.* **2017**, *7*, 15753.

(31) Bao, Y.-W.; Hua, X.-W.; Li, Y.-H.; Jia, H.-R.; Wu, F.-G. *ACS Appl. Mater. Inter.* **2018**, *10*, 1544-1555.

(32) Qiao, Y.; Gumin, J.; MacLellan, C. J.; Gao, F.; Bouchard, R.; Lang, F. F.; Stafford, R. J.; Melancon, M. P. *Nanotechnology* **2018**, *29*, 165101.

(33) Ge, J.; Jia, Q.; Liu, W.; Guo, L.; Liu, Q.; Lan, M.; Zhang, H.; Meng, X.; Wang, P. *Adv. Mater.* **2015**, *27*, 4169-4177.

(34) Cheng, L.; Liu, J.; Gu, X.; Gong, H.; Shi, X.; Liu, T.; Wang, C.; Wang, X.; Liu, G.; Xing, H.; Bu, W.; Sun, B.; Liu, Z. *Adv. Mater.* **2014**, *26*, 1886-1893.

(35) Lyu, Y.; Pu, K. *Adv. Sci.* **2017**, *4*, 1600481.

(36) Miao, Q.; Pu, K. *Bioconjugate Chem.* **2016**, *27*, 2808-2823.

(37) Zhang, J.; Zhen, X.; Upputuri, P. K.; Pramanik, M.; Chen, P.; Pu, K. *Adv. Mater.* **2017**, *29,* 1604764.

(38) Zhang, J.; Hu, J.; Sang, W.; Wang, J.; Yan, Q. *ACS Macro Lett.* **2016**, *5*, 919-924.

(39) Pham, W.; Cassell, L.; Gillman, A.; Koktysh, D.; Gore, J. C. *Chem. Commun.* **2008**, 1895-1897.

(40) Miao, Q.; Yeo, D. C.; Wiraja, C.; Zhang, J.; Ning, X.; Xu, C.; Pu, K. *Angew. Chem.* **2018**, *130*, 1270-1274.

(41) Luo, Z.; Huang, Z.; Li, K.; Sun, Y.; Lin, J.; Ye, D.; Chen, H.-Y. *Anal. Chem.* **2018**, *90*, 2875-2883.

(42) Zhang, J.; Wang, J.; Liu, J.; Ning, L.; Zhu, X.; Yu, B.; Liu, X.; Yao, X.; Zhang, H. *Anal. Chem.* **2015**, *87*, 4856-4863.

(43) Zhang, J.; Li, C.; Zhang, R.; Zhang, F.; Liu, W.; Liu, X.; Lee, S. M.-Y.; Zhang, H. *Chem. Commun.* **2016**, *52*, 2679-2682.

(44) Zhen, X.; Zhang, J.; Huang, J.; Xie, C.; Miao, Q.; Pu, K. *Angew. Chem. Int. Ed.* **2018**, DOI: 10.1002/anie.201803321.

(45) Szabó, C.; Ischiropoulos, H.; Radi, R. *Nat. Rev. Drug Discov.* **2007**, *6*, 662-680.

(46) Lyu, Y.; Fang, Y.; Miao, Q.; Zhen, X.; Ding, D.; Pu, K. *ACS Nano* **2016**, *10*, 4472-4481.

(47) Lyu, Y.; Xie, C.; Chechetka, S. A.; Miyako, E.; Pu, K. *J. Am. Chem. Soc.* **2016**, *138*, 9049-9052.

(48) Pu, K.; Mei, J.; Jokerst, J. V.; Hong, G.; Antaris, A. L.; Chattopadhyay, N.; Shuhendler, A. J.; Kurosawa, T.; Zhou, Y.; Gambhir, S. S.; Bao, Z.; Rao, J. *Adv. Mater.* **2015**, *27*, 5184-5190.

(49) Jiang, Y.; Pu, K. *Small* **2017**, *13*, 1700710.

(50) Yin, C.; Zhen, X.; Fan, Q.; Huang, W.; Pu, K. *ACS Nano* **2017**, *11*, 4174-4182.

(51) Yin, C.; Zhen, X.; Zhao, H.; Tang, Y.; Ji, Y.; Lyu, Y.; Fan, Q.; Huang, W.; Pu, K. *ACS Appl. Mater. Inter.* **2017**, *9*, 12332-12339.

For TOC only